ARL-TR-8886 ● JAN 2020

Defect Characterization in Silicon Carbide by Cathodoluminescence

by Harun Gopal Ganesan, Robin Karhu, and Brenda VanMil

NOTICES

Disclaimers

ARL-TR-8886 ● JAN 2020

Defect Characterization in Silicon Carbide by Cathodoluminescence

Harun Gopal Ganesan
Science and Engineering Apprenticeship Program (SEAP)

Robin Karhu
Oak Ridge Associated Universities (ORAU) Maryland

Brenda VanMil
Sensors and Electron Devices Directorate, CCDC Army Research Laboratory

REPORT DOCUMENTATION PAGE						*Form Approved* *OMB No. 0704-0188*
Public reporting burden for this collection of information is estimated to average 1 hour per response, including the time for reviewing instructions, searching existing data sources, gathering and maintaining the data needed, and completing and reviewing the collection information. Send comments regarding this burden estimate or any other aspect of this collection of information, including suggestions for reducing the burden, to Department of Defense, Washington Headquarters Services, Directorate for Information Operations and Reports (0704-0188), 1215 Jefferson Davis Highway, Suite 1204, Arlington, VA 22202-4302. Respondents should be aware that notwithstanding any other provision of law, no person shall be subject to any penalty for failing to comply with a collection of information if it does not display a currently valid OMB control number. **PLEASE DO NOT RETURN YOUR FORM TO THE ABOVE ADDRESS.**						
1. REPORT DATE *(DD-MM-YYYY)* January 2020		**2. REPORT TYPE** Technical Report				**3. DATES COVERED (From - To)**
4. TITLE AND SUBTITLE Defect Characterization in Silicon Carbide by Cathodoluminescence						**5a. CONTRACT NUMBER**
						5b. GRANT NUMBER
						5c. PROGRAM ELEMENT NUMBER
6. AUTHOR(S) Harun Gopal Ganesan, Robin Karhu, and Brenda VanMil						**5d. PROJECT NUMBER**
						5e. TASK NUMBER
						5f. WORK UNIT NUMBER
7. PERFORMING ORGANIZATION NAME(S) AND ADDRESS(ES) CCDC Army Research Laboratory ATTN: FCDD-RLS-EM Adelphi, MD 20783-1138						**8. PERFORMING ORGANIZATION REPORT NUMBER** ARL-TR-8886
9. SPONSORING/MONITORING AGENCY NAME(S) AND ADDRESS(ES)						**10. SPONSOR/MONITOR'S ACRONYM(S)**
						11. SPONSOR/MONITOR'S REPORT NUMBER(S)
12. DISTRIBUTION/AVAILABILITY STATEMENT Approved for public release; distribution is unlimited.						
13. SUPPLEMENTARY NOTES ORCID ID(s): Brenda VanMil, https://orcid.org/0000-0003-1659-4379; Robin Karhu, https://orcid.org/0000-0003-4691-5647						
14. ABSTRACT During homoepitaxial growth of silicon carbide (SiC), structural defects propagate from the substrate into the growing epitaxial layer. Locating and characterizing these defects are key to assessing the quality of the material and understanding the influence of the defects on device properties. Cathodoluminescence (CL) imaging has been reported to nondestructively locate defects in gallium nitride (GaN) by observing the lower intensity of the band edge CL. Similar to GaN, the structural defects in SiC may work as recombination paths for minority carriers and may exhibit a similar behavior. The literature has not shown use of CL to locate linear defects, such as basal place dislocations, threading edge dislocations, or threading screw dislocations for SiC. It is expected to be more difficult to locate defects in SiC compared to GaN due to the far lower density of defects (~10^3 vs. ~10^4–10^6 cm^{-3}). This study investigates CL as an alternative method to locate and identify linear, planar, and morphological structural defects in 4H-SiC in a nondestructive manner. This is accomplished through CL mapping followed by a destructive defect etch to confirm the locations of defects. Improvements to the equipment and approach are discussed for follow-up work to this study.						
15. SUBJECT TERMS silicon carbide, cathodoluminescence, linear defects, threading edge dislocations, stacking faults						
16. SECURITY CLASSIFICATION OF:			**17. LIMITATION OF ABSTRACT**	**18. NUMBER OF PAGES**		**19a. NAME OF RESPONSIBLE PERSON** Brenda VanMil
a. REPORT Unclassified	**b. ABSTRACT** Unclassified	**c. THIS PAGE** Unclassified	UU	20		**19b. TELEPHONE NUMBER (Include area code)** (301) 394-0979

Standard Form 298 (Rev. 8/98)
Prescribed by ANSI Std. Z39.18

Contents

List of Figures	**iv**
1. Introduction/Background	**1**
2. Experiment	**2**
3. Results/Discussion	**5**
4. Conclusion	**11**
5. References	**12**
List of Symbols, Abbreviations, and Acronyms	**13**
Distribution List	**14**

List of Figures

Fig. 1 Comparison of the as-grown and etched sample of SiC demonstrating how the TDs were used for image alignment 3

Fig. 2 Microscope images after KOH etching for a) 5 min 450 °C, b) 10 min 450 °C, c) 5 min 500 °C, and d) 10 min 500 °C 4

Fig. 3 The 4° off-axis 4H-SiC epitaxial layer etched for 10 min at 500 °C. Examples of a TED, SD BPD, and TD are all seen in this micrograph.4

Fig. 4 Comparison of the optical microscopy, post-etch optical microscopy, SEM imaging, and CL imaging, for the sample area denoted as TD1. The circled areas show contrast in the CL intensity within the SF where TEDs are located. 5

Fig. 5 Comparison of the optical microscopy, post-etch optical microscopy, SEM imaging, and CL imaging for the sample area denoted as TD2. The circled area shows contrast in the CL intensity within the SF where TEDs are located. 6

6

Fig. 6 Comparison of the optical microscopy, post-etch optical microscopy, SEM imaging, and CL imaging for the sample denoted as TD3 6

Fig. 7 Comparisons of the optical microscopy, post-etch optical microscopy, SEM imaging, and CL imaging for the sample areas denoted as TD4 and TD5 7

Fig. 8 Comparison of the optical microscopy, post-etch optical microscopy, SEM imaging, and CL imaging for the area on the sample denoted as TD6 8

Fig. 9 Comparison of the optical microscopy, post-etch optical microscopy, SEM imaging, and CL imaging for the area on the sample denoted as TD7 8

Fig. 10 Comparison of the optical microscopy, post-etch optical microscopy, SEM imaging, and CL imaging for the area on the sample denoted as TD8 9

Fig. 11 The position of each spot can be observed in an SEM image taken of an area that had a CL image taken previously 10

1. Introduction/Background

Silicon carbide (SiC) is a wide-bandgap semiconductor used primarily for power and opto-electronic devices. During homoepitaxial growth of SiC, structural defects propagate from the substrate into the growing epitaxial layer. These defects affect the properties of the material, for example, they work as a recombination path for minority charge carriers.[1,2] Locating and characterizing these defects are key to assessing the quality of the material and understanding the influence of the defects on device properties. Some of these linear structural defects intersect the surface of the epitaxial layer; these include basal plane dislocations (BPDs), threading screw dislocations (TSDs), threading edge dislocations (TEDs), and micropipes. TSDs, TEDs, and micropipes propagate along the c-axis. BPDs propagate perpendicular to the c-axis and intersect the surface due to the offcut (surface normal is not parallel to the c-axis) used to replicate the substrate polytype into the growing epitaxial layer. Due to the polymorphic nature of SiC, where different polytypes exist as different stacking sequences of Si-C bilayers, the formation energy of structural defects is very low.[3] This report investigates the hexagonal polytype known as 4H-SiC. When a different stacking sequence occurs as a planar defect in the 4H polytype, it is called a stacking fault (SF). Due to the offcut of the sample, the planar defects also intersect with the surface. A triangular defect (TD) can also be created from a particle (downfall) or a micropipe. These defects can be a polytype inclusion or a complex of SFs that is readily visible in the surface morphology.

There exist several methods to locate structural defects in SiC, including etching in molten potassium hydroxide (KOH), X-ray topography, μ-photoluminescence, and electron-beam induced current (EBIC).[4–6] Of these, the methods readily available for locating defects at the US Army Combat Capabilities Development Command Army Research Laboratory (ARL) at Adelphi, Maryland, are KOH etching and EBIC. KOH etching is a destructive method for locating and identifying defects, and EBIC requires some sample preparation.

Cathodoluminescence (CL) is a process in which the sample is illuminated with a beam of electrons at one point. The sample reacts to this by emitting light at a certain wavelength and intensity. Albrecht et al.[4] reported using CL imaging to nondestructively locate defects in gallium nitride (GaN) by observing the lower intensity of the band edge CL. CL in GaN is nondestructive, requires minimal setup, and is relatively fast. Similar to GaN, the structural defects in SIC may work as recombination paths for minority carriers and may exhibit a similar behavior.

Maximenko et al.[7] reported CL of SFs in SiC epilayers; however, the literature has not shown use of CL to locate linear defects, such as BPDs, TEDs, and TSDs, for

SiC. It is expected to be more difficult to locate defects in SiC compared to GaN due to the far lower density of defects (~10^3 vs. ~10^4–10^6 cm^{-3}).[8–9] The use of EBIC has been used to show the locations of line dislocations, such as TEDs and TSDs.[2] ARL currently has an scanning electron microscope (SEM) equipped with both EBIC and CL. If it is possible to identify defects using CL in SiC, the eventual goal is to then correlate the defects in CL and EBIC.

This study investigates CL as an alternative method to locate and identify structural defects in 4H-SiC in a nondestructive manner, with minimal sample preparation, and performed with equipment readily available at ARL.

This initial study was conducted over 10 weeks during the summer of 2019 under the Science and Engineering Apprenticeship Program.

2. Experiment

A sample from a 20-µm-thick epitaxial layer grown on an N+ 4H-SiC substrate with numerous triangular defects was chosen for this experiment to facilitate sample location alignment in images. Note that this sample had been irradiated with 7.5-kGy, 2-MeV electrons. Microscope images were taken using a Leica DM2700 microscope and large-area images were taken using Leica software multistep image stitching.

CL images were taken using a CamScan SEM operating with a 20-keV accelerating voltage and a nominal 100-µA electron beam emission current with an attached Applied Beams (Beaverton, Oregon) CL system. The CL signal is gathered from a parabolic mirror, which is then either separated by wavelength using a diffraction grating for monochromatic measurements or reflected by a mirror for panchromatic measurements over a wavelength range of 190 to 850 nm. The photons are measured using a charge-coupled device (CCD) camera. CL images were taken near unique in-grown SFs to ensure that the area on the sample could be found again after defect etching, as demonstrated by a comparison of an as-grown and post-etch image shown in Fig. 1. After the etch condition was finalized, the imaged sample was etched at the optimal condition to reveal surface defects. Multiple optical images were taken of the sample at the same locations where the CL was previously taken. Then, the CL images were compared to the respective optical image of the etched sample.

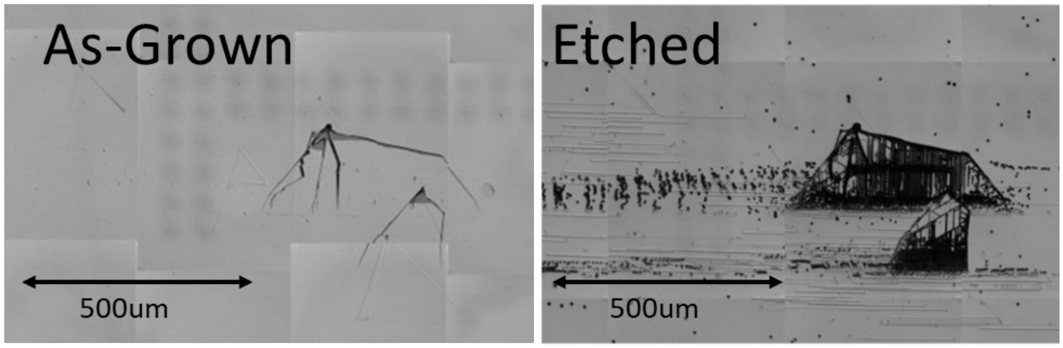

Fig. 1 Comparison of the as-grown and etched sample of SiC demonstrating how the TDs were used for image alignment

The KOH etching conditions were optimized for our experimental setup. Samples were etched in a nickel wire basket. Molten KOH was contained within a nickel crucible. Four different test samples, all from the same wafer, were etched at different temperatures and durations. The different samples were etched for 5 min at 450 °C, 10 min at 450 °C, 5 min at 500 °C, and 10 min at 500 °C (Fig. 2, left to right, respectively). After etching, samples cooled in air and were then rinsed in flowing deionized (DI) water. Each etch condition produced different sized etch pits, as seen in Fig. 2. For this experiment, it was determined that etching for 5 min at 500 °C was optimal because it clearly revealed the four main types of defects shown in Fig. 3, while also not over-etching the sample. These defects shown are consistent with those shown by Kimoto and Cooper.[10] Over-etching can lose definition, making it difficult to differentiate between the types of defects.

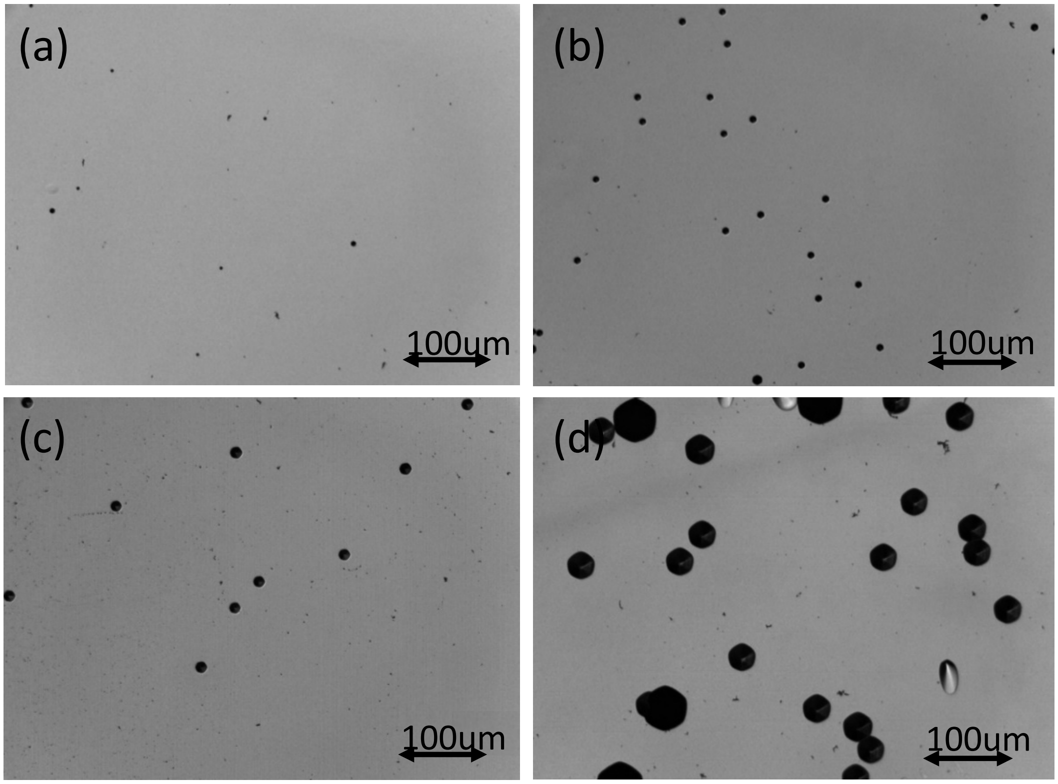

Fig. 2 Microscope images after KOH etching for a) 5 min 450 °C, b) 10 min 450 °C, c) 5 min 500 °C, and d) 10 min 500 °C

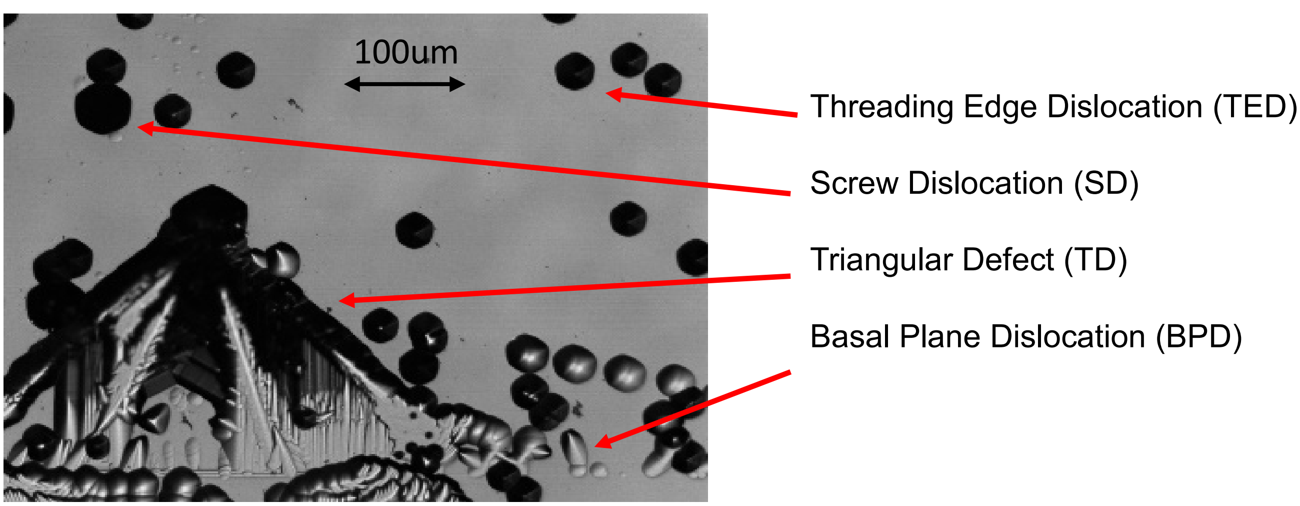

Fig. 3 The 4° off-axis 4H-SiC epitaxial layer etched for 10 min at 500 °C. Examples of a TED, SD BPD, and TD are all seen in this micrograph.

3. Results/Discussion

A total of eight regions near TDs were imaged in this study. Each sequence is shown in Figs. 4–10 and proceeds from left to right with an as-grown microscope image; the post-etch microscope image; the SEM image, which includes the area acquired with CL imaging; and then finally, the CL image itself. For TD1, TD2, and TD8, a small CL-imaged area overlays the SEM image. A red box is used to indicate the area acquired with the CL image.

The CL, SEM, and corresponding pre- and post-etch optical images of the etched sample at the same location for each area clearly display the TDs. TDs that have been revealed by etching are shown in the CL image through an area of increased or decreased intensity relative to the background. All TDs imaged by the microscope in this investigation were discernable in the CL.

In Fig. 4, the CL image for TD1 indicated by the yellow oval and labeled A is within the TD. The area, labeled B, is outside of the TD, but inside of a SF. The pre-etch CL has contrast in the areas that contain TEDs within the SF.

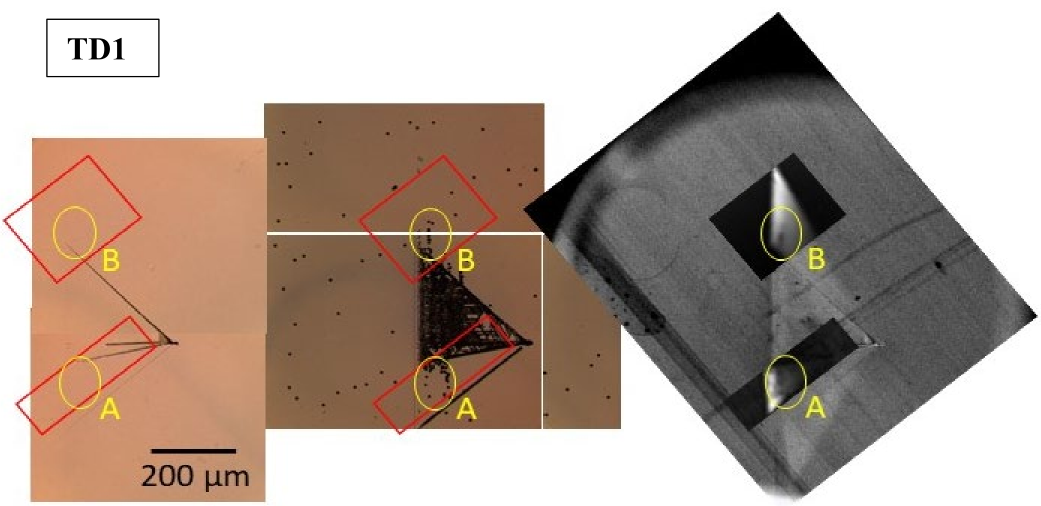

Fig. 4 Comparison of the optical microscopy, post-etch optical microscopy, SEM imaging, and CL imaging, for the sample area denoted as TD1. The circled areas show contrast in the CL intensity within the SF where TEDs are located.

The small-area CL image for TD2, shown in Fig. 5, centered at the point of the TD does not have any contrast differentiation and the etch pit microscope image corresponding to that area does not include any etch pits. The large-area CL image does contain some contrast in the area within the oval inside the SF, outside the TD. There is no contrast observed for the TEDs outside of the SF.

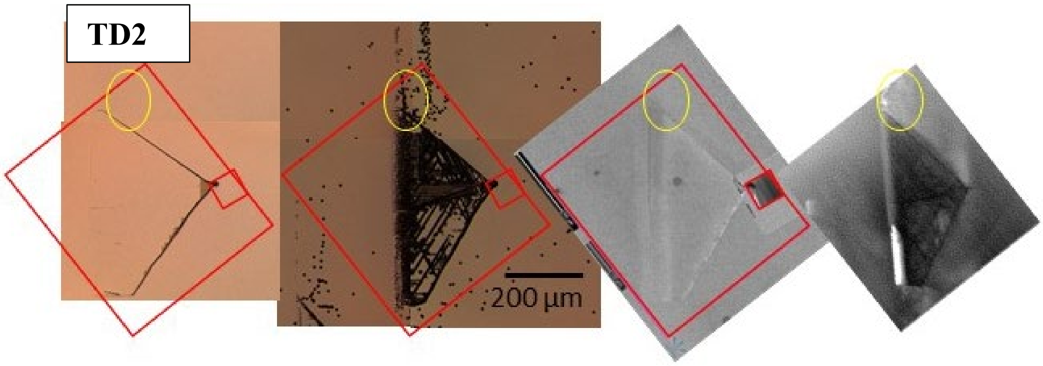

Fig. 5 Comparison of the optical microscopy, post-etch optical microscopy, SEM imaging, and CL imaging for the sample area denoted as TD2. The circled area shows contrast in the CL intensity within the SF where TEDs are located.

The CL images for TD3, TD4, and TD5, in Figs. 6 and 7, show the nucleating defect for the TD. However, there is no contrast for the numerous TEDs that are observed within the area on the etch pit microscope image.

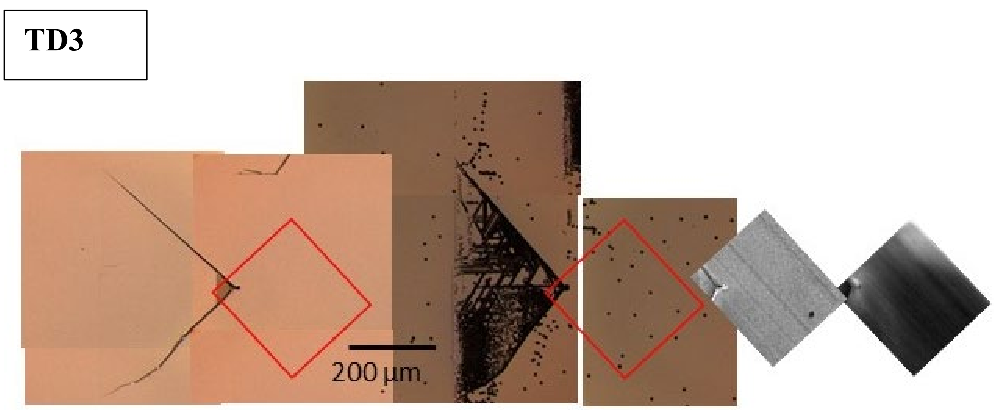

Fig. 6 Comparison of the optical microscopy, post-etch optical microscopy, SEM imaging, and CL imaging for the sample denoted as TD3

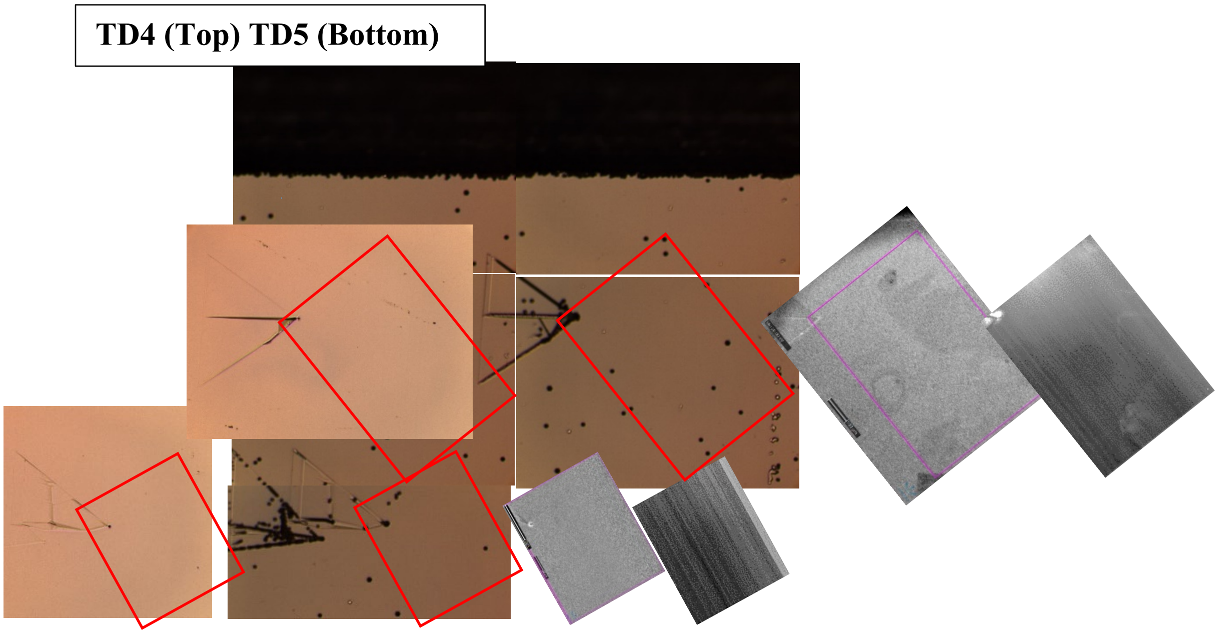

Fig. 7 Comparisons of the optical microscopy, post-etch optical microscopy, SEM imaging, and CL imaging for the sample areas denoted as TD4 and TD5

The CL image for TD6, in Fig. 8, was taken in area with a high density of in-grown SFs. There are also a large quantity of defects that are associated with the SFs that nucleated from the TD at the bottom of the image. These TEDs are apparent in the 420- and 465-nm monochromatic CL images.

The CL image for TD7, in Fig. 9, is also taken in an area with a TD and a high density of in-grown SFs.

TD6

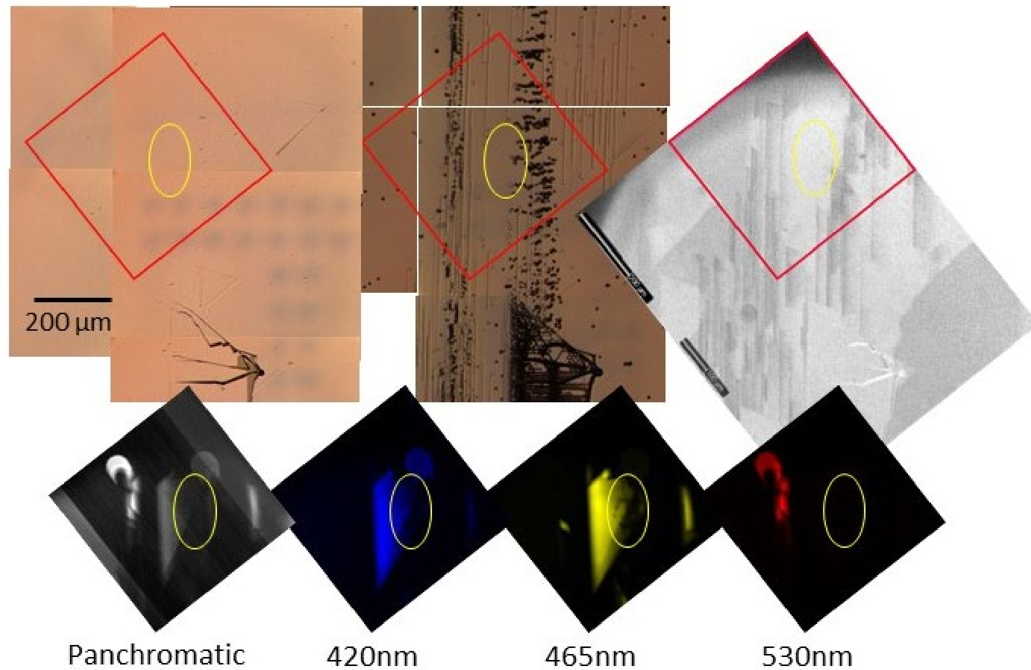

Fig. 8 Comparison of the optical microscopy, post-etch optical microscopy, SEM imaging, and CL imaging for the area on the sample denoted as TD6

TD7

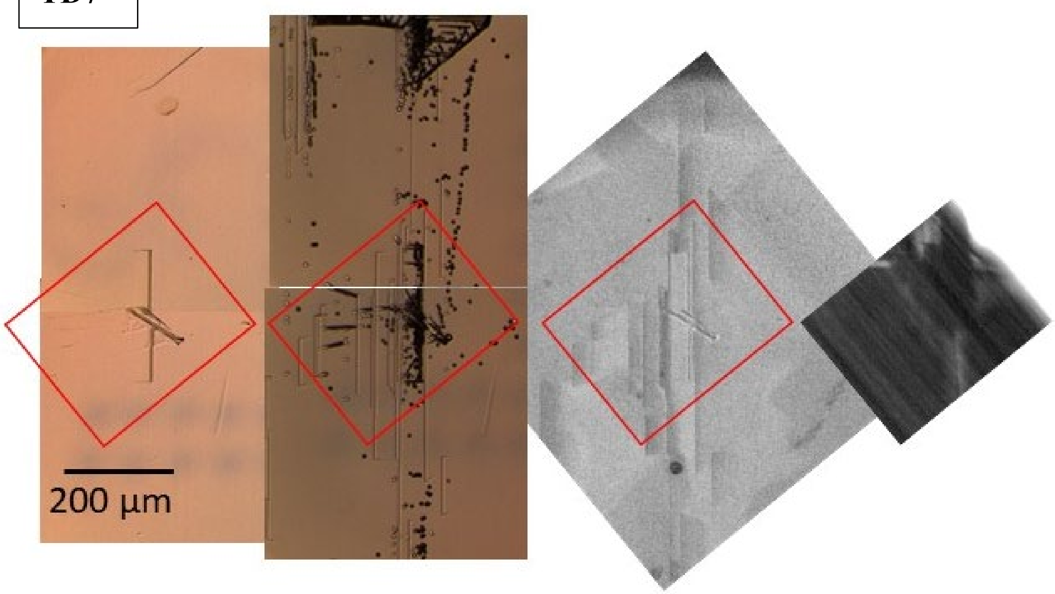

Fig. 9 Comparison of the optical microscopy, post-etch optical microscopy, SEM imaging, and CL imaging for the area on the sample denoted as TD7

There are observations where the CL also indicates planar defects not revealed by defect etching. These cases are the same as the SFs in SiC imaged by Maximenko et al.[7] Etching only reveals defects where they intersect with the surface, while CL can also reveal planar defects within the material. In the image for TD8, in Fig. 10, the CL clearly indicates a SF in the yellow oval location; however, the SF is not fully observed in the etched sample. This is because the SF is below the surface of the sample and, therefore, not visible in the etched sample. Note that the SF observed in the CL but not the optical microscope are also observed in the SEM image. The smaller circles in TD8 indicate the presence of BPDs. These BPDs demarcate the edges of partial dislocations, which coincide with the boundaries of in-grown SFs. CL imaging and SEM are methods to determine the location and size of in-grown SFs. In-grown SFs are also observed in TD1, TD2, TD6, and TD7.

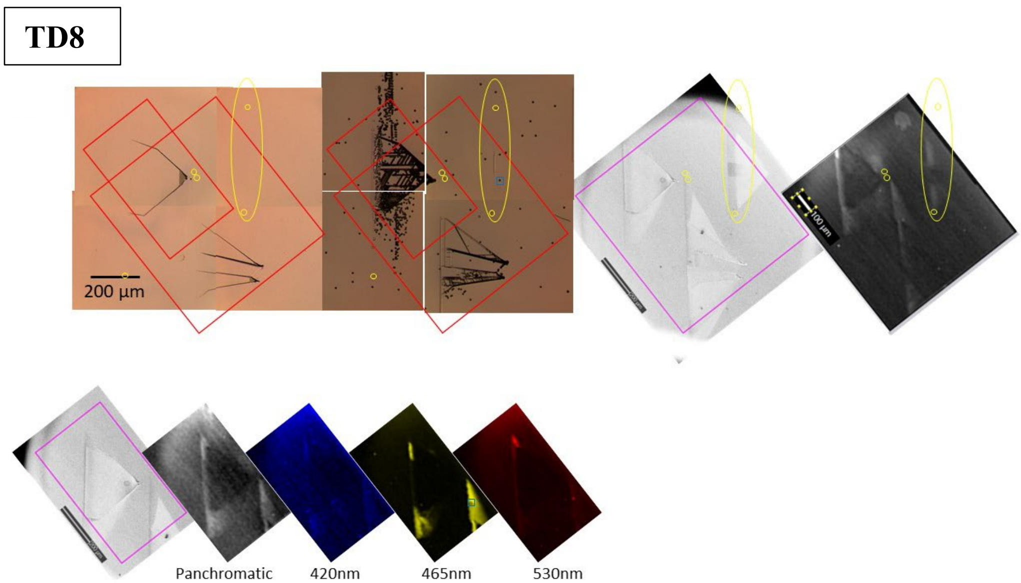

Fig. 10 Comparison of the optical microscopy, post-etch optical microscopy, SEM imaging, and CL imaging for the area on the sample denoted as TD8

Two of the areas (TD6 and TD8) also include a comparison of the panchromatic CL image to monochromatic CL imaging at three peak wavelengths of 420, 465, and 530 nm. These wavelengths were chosen by finding peaks in a spectral plot taken within TD6. These wavelengths are all reported with discussion of the types of SFs in Maximenko et al.[7] Different wavelengths of CL imaging can reveal multiple types of SFs. Different types of SFs emit different wavelengths of light, as seen in TD6 and TD8. This indicates there are multiple SFs in the same area existing on different planes.

After the sample was etched, CL was again obtained for TD1, TD2, and TD7 to determine the likely wavelength band in the panchromatic CL from the in-grown

SF. Monochromatic post-etch CL was performed on both TD1A and TD2B post-etch indicating the emission centered at 505 nm for area A and 465 nm for area B was responsible for revealing contrast at areas containing TEDs. The monochromatic post-etch CL emission for TD2 is broad around 530 nm. The monochromatic post-etch CL emission for TD7 had peaks near 460 and 505 nm depending on the underlying SF.

For this study, the highest-resolution CL was not selected because of the time needed to acquire the images. The resolution of the CL scans is likely not sufficient to observe some defects in the SEM scans. This was learned when an SEM image was acquired in the same location after a CL image was taken and the spot scans left a pattern in the sample (possibly due to charging or carbon deposition). This is seen in Fig. 11. Optimization of the SEM spot size and the resolution need to be performed to ensure all areas of the sample are imaged by the CL. The time issue limiting the resolution can be addressed by upgrading the detector from a CCD to a photo multiplier tube (PMT) detector.

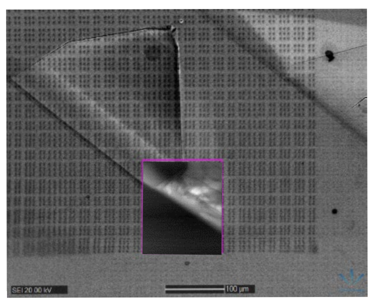

Fig. 11 The position of each spot can be observed in an SEM image taken of an area that had a CL image taken previously

This initial work indicates that the wavelength range of the CL is important for observing the decreased intensity of the CL due to the presence of defects in SiC. As noted for the GaN, the band edge CL was imaged for determining the position of dislocations. This study focused on acquisition of panchromatic CL due to the weak band edge emission in this sample. In this study, dislocations were observed in areas with a brighter CL from in-grown SFs. The weak band edge CL in this SiC sample, coupled with the noise from the CCD, did not allow for imaging of defects in regions without SFs, if that is possible.

4. Conclusion

A combination of the low density of defects in areas without SFs, incomplete coverage of the CL scans, and the low intensity of the band edge emission are potentially contributing factors as to why a decrease in intensity associated with observation of defects by CL was not obtained in this study. It is recommended that 1) the CL collection procedures be refined to obtain CL from all areas of the sample, 2) the CCD be replaced with a PMT, and 3) a sample with higher band edge CL be obtained to determine the feasibility of this method.

5. References

1. Feng G, Suda J, Kimoto T. Nonradiative recombination at threading dislocations in 4H-SiC epilayers studied by micro-photoluminescence mapping. Journal of Applied Physics. 2011;110(3).

2. Maximenko SI, Freitas JA, Myers-Ward RL, Lew KK, VanMil BL, Eddy CR, Gaskill DK, Muzykov PG, Sudarshan TS. Effect of threading screw and edge dislocations on transport properties of 4H–SiC homoepitaxial layers. Journal of Applied Physics. 2010;108(1).

3. Hong MH, Samant AV, Pirouz P. Stacking fault energy of 6H-SiC and 4H-SiC single crystals. Philosophical Magazine A. 2000;80(4):919–935.

4. Albrecht M, Weyher JL, Lucznik B, Grzegory I, Porowski S. Nonradiative recombination at threading dislocations in n-type GaN: studied by cathodoluminescence and defect selective etching. Applied Physics Letters. 2008;92(23).

5. Chen B, Chen J, Sekiguchi T, Kinoshita A, Matsuhata H, Yamaguchi H, Nagai I, Okumur H. Electron-beam-induced current study of electrical activity of dislocations in 4H–SiC homoepitaxial film. Journal of Materials Science: Materials in Electronics. 2008;19(S1):219–223.

6. Ohno T, Yamaguchi H, Kuroda S, Kojima K, Suzuki T, Arai K. Direct observation of dislocations propagated from 4H–SiC substrate to epitaxial layer by X-ray topography. Journal of Crystal Growth. 2004;260(1–2):209–216.

7. Maximenko SI, Freitas JA, Klein PB, Shrivastava A, Sudarshan TS. Cathodoluminescence study of the properties of stacking faults in 4H-SiC homoepitaxial layers. Applied Physics Letters. 2009;94(9).

8. Yoshida T, Oshima Y, Eri T, Ikeda K, Yamamoto S, Watanabe K, Shibata M, Mishima T. Fabrication of 3-in GaN substrates by hydride vapor phase epitaxy using void-assisted separation method. Journal of Crystal Growth. 2008;310(1):5–7.

9. Suihkonen S, Pimputkar S, Sintonen S, Tuomisto F. Defects in single crystalline ammonothermal gallium nitride. Advanced Electronic Materials. 2017;3(6).

10. Kimoto T, Cooper JA. Fundamentals of silicon carbide technology: growth, characterization, devices and applications. New York (NY): Wiley; 2014.

List of Symbols, Abbreviations, and Acronyms

BPD	basal plane dislocation
CCD	charge-coupled device
CL	cathodoluminescence
EBIC	electron beam induced current
GaN	gallium nitride
KOH	potassium hydroxide
PMT	photo multiplier tube
SEM	scanning electron microscope
SF	stacking fault
SiC	silicon carbide
TD	triangular defect
TED	threading edge dislocation
TSD	threading screw dislocation

1 (PDF)	DEFENSE TECHNICAL INFORMATION CTR DTIC OCA
1 (PDF)	CCDC ARL FCDD RLD CL TECH LIB
1 (PDF)	CCDC ARL FCDD RLS EM B VANMIL